 CMES, vol.4, no.1, pp.177-196, 2003

Analysis of Materials with Strain-Gradient Effects: A Meshless Local Petrov-Galerkin(MLPG) Approach, with Nodal Displacements only

Z.Tang, S. Shen and S.N. Atluri[1]

Abstract: A meshless numerical implementation is reported of the 2-D Fleck-Hutchinson phenomenological strain-gradient theory, which fits within the framework of the Toupin-Mindlin theories and deals with first-order strain gradients and the associated work-conjugate higher-order stresses. From a mathematical point of view, the two-dimensional Toupin-Mindlin strain gradient theory is a generalization of the Poisson-Kirchhoff plate theories, involving, in addition to the fourth-order derivatives of the displacements, also a second-order derivative. In the conventional displacement-based approaches in FEM, the interpolation of displacement requires C^1 –continuity (in order to ensure convergence of the finite element procedure for 4^{th} order theories), which inevitably involves very complicated shape functions. These shape functions involve large numbers of degrees of freedom in every element, including nodal displacements, nodal rotations (i.e. first order gradients of displacement), and even higher order derivatives. C^1-continuous methods are mostly feasible only for one-dimensional problems. The standard approach for solving Bernoulli-Euler beam problems is by employing C^1-continuous Hermite cubic shape functions, interpolating both displacements and rotations (i.e., slopes). For two-dimensional problems, such as involving plate and shell analysis, C^1-continuous methods are very complicated, and formulations for three-dimensional problems as they arise from strain gradient theories become more or less intractable. The high computational cost and large number of degrees of freedom soon place such formulations beyond the realm of practicality. Recently some mixed and hybrid formulations, requiring only C^0-continuity, have also been developed and applied to strain gradient plasticity or elasticity problems. But they are even more problematic. While some of the developed elements have been subjected to the Patch test and other benchmark problems, a rigorous numerical analysis is missing: mathematical proofs of consistency and stability have not been demonstrated, and the rate of convergence has not been established. The large number of nodal degrees of freedom is still inevitable in such mixed methods. It is evident that currently, no efficient finite element methods are available for strain gradient theory formulations.
In this paper, a truly meshless approach, the Meshless Local Petrov-Galerkin Method(MLPG), is introduced for higher-order gradient theories that trace their roots to the work of Toupin. The degrees of freedom consist of only nodal displacements, i.e. nodal rotational degrees of freedom are not used. A numerical analysis of the method is presented, covering the usual ground of consistency, stability and hence, convergence in several examples. All the results show that, when solving fourth-order elliptic problems such as those arising in gradient theories of material behavior, the MLPG method is superior to primal or mixed finite element procedures.

keyword: MLPG, Gradient theory, MLS

1 Introduction

The most widely used theories of continuum solid mechanics involve non-polar materials that are also simple in the sense of Noll (1965). Material point rotations are neglected, and the Cauchy stress is assumed to be a functional of the deformation, only through its first gradient. This local assumption has, for long, proved to be adequate when the wavelength of a deformation field is much larger than the dominant microstructural length scale of the material. However, when the two length scales are comparable, this assumption is questionable. An interest in polar materials has existed at least since the pioneering work of the Cosserats(1907,1909). The rotational degrees of freedom introduce couple stresses and body couples. Rich theories of

[1] Center for Aerospace Research and Education,
University of California, Irvine
5251 California Ave, Suite 140
Irvine, CA 92612, USA

such continua were worked out in the 1960s(Truesdell & Toupin 1960, Toupin 1962, Mindlin 1964) The terms "micropolar" and "micromorphic" continua were coined to refer to solids in which the directors attached to material points are respectively rigid and deformable (Eringen, 1976). Such theories have applications in electrically polarized media, granular materials and in biological tissues, among other areas. Since they introduced a length scale, "Cosserat continua" have been proposed as regularized descriptions of softening materials (Borst & Sluys, 1991), which otherwise demonstrate deformations localized onto bands of vanishing width.

The earliest work involving higher-order gradients of deformation appears to be that of Cauchy (1851). Such continua were termed "materials of grade n" by Truesdell and Noll(1965), referring to the order of the highest derivative of the deformation. Linear and nonlinear elasticity were considered, in light of the role played by the second gradient of displacement, i.e., the strain gradient, by Truesdell and Toupin (1960), and later by Toupin (1962). The balance laws included a higher-order stress—"couple stress" in this case, and hence required higher-order boundary conditions on the "couple stress" traction and strain. Assuming a stored energy function, the couple stress was related, via formal procedures, to the strain gradient. Shortly after that, Mindlin (1964) proposed a linear theory that encompassed the theories of the Cosserats and of Toupin as special cases. The formalism of Toupin and Mindlin was recently extended to the deformation and flow theories of plasticity (Fleck & Hutchinson, 1997), motivated by some experimental observations of the apparent length scale dependence of plasticity in metals, when deformations vary at scales of the order of a micron (Stelmashenko et al, 1993; Fleck et al. 1994; Stolken et al, 1998). Variants of this strain gradient plasticity theory have also appeared (Gao et al, 1999; Huang et al, 2000; Chen et al, 2002). These theories have been widely applied to studying length scale-dependent deformation phenomena in metals. Polar and higher-order continuum theories have been applied to layered materials, composites and granular media, in addition to polycrystalline metals.

The solution of the initial and boundary value problems posed in terms of the higher-order theories is not straightforward: the governing differential equation and boundary conditions are complicated (Toupin, 1962) and analytic solutions are restricted to the simplest cases. Computational difficulties also arise. While boundary conditions are easier to treat in the variational setting, requirements of regularity dictate that, in FEM the displacement must be a C^1 function over the domain. The degrees of freedom include nodal displacements and displacement gradients. The situation is partially analogous to classical Bernoulli-Euler beam and Poisson-Kirchhoff plate theories in one and two spatial dimensions respectively.

Finite element formulations incorporating C^1 displacement fields are therefore a natural first choice for strain gradient theories. For example, the use of Specht's triangular element (Specht, 1988) for the special case of couple stress theory was examined (Xia & Hutchinson, 1996). The element contains displacement derivatives as extra nodal degrees of freedom(denoted as DOF subsequently), and C^1-continuity is satisfied only in a weak averaged sense along each side of the element; therefore, the element is not a strict C^1 element. Furthermore, the element fails to deliver an accurate pressure distribution for an incompressible, non-linear solid (Xia & Hutchinson, 1996). There is a reliable rectangular C^1 element (Zienkiewicz and Taylor, 1994), but its shape and numbers of DOF are obviously strong limitations.

The lack of robust C^1-continuous elements then drove the development of various C^0-continuous elements for couple stress theory in last decades (Herrmann, 1983; Xia & Hutchinson, 1996; Shu & Fleck, 1998; Shu et al. 1999, Amanatidou & Aravas, 2002; Engel et al. 2002; Tenek and Aifantis 2002; etc.). Finite element formulations for the Fleck-Hutchinson strain gradient plasticity theory have been developed with plate elements as a basis, but were generally found to perform poorly (Xia & Hutchinson, 1996). Mixed and hybrid formulations have also been developed in the same work and elsewhere: Shu et al(1999) introduced some C^0 element types, where nodal degrees of freedom include nodal displacements and corresponding gradients, and kinematic constraints between displacement gradients are enforced via the Lagrange multiplier method. Their lowest-order triangular element requires 28 unknowns per element, and their lowest-order quadrilateral element 38 unknowns; Amanatidou and Aravas(2002) proposed mixed C^0-contiunity finite element formulations, where every element includes around 70 nodal degrees of freedom in 2-D problems. From these numbers it is evident that currently, no efficient finite element methods are available for strain gradient theory formulations.

The importance of the role of a rotation-free approximation has been realized for a long time, especially when solving problems involving high order PDE. For example, in the thin-plate bending theories, if there is no need for independent rotation fields, it is consequently possible to develop methods that do not involve rotational degrees of freedom. Basically this spirit was well established in finite difference formulations (Timoshenko, 1959), but finite element counterparts to this idea seemed impossible due to the necessity of employing slope degrees of freedom in order to satisfy continuity requirements. In the last decade, a number of procedures has been proposed(Babuka and Zlámal 1973; Baker 1977; Phaal and Calladine 1992a, 1992b; Oñate and Cervera 1993; Oñate and Zarate, 2000), based on a combination of finite difference, finite element, finite volume and ad hoc concepts, leading to elements with only displacement degrees of freedom. Typically, these elements are very simple, i.e. the three-node triangle has dominated, and they all involve non-locality. By non-locality we mean that the curvature in an element depends on the displacement field in that element and its neighbors. Consequently, these elements fall outside the classical framework. Furthermore, C^1-continuity requirements are simply ignored (for the most part, elements of this type are viewed pejoratively: they are frequently described as non-conforming, incompatible, and variational crimes (Strang et al, 1973)), but these elements seem to perform fairly well and have the great advantage of eliminating altogether the rotational degrees of freedom. In the linear case, this leads to a saving of computer solution time and in the non-linear case it additionally amounts to a substantial reduction in complexity. The reason for this is that, in the linear case, rotations have a vector space structure (i.e., R3), whereas in the non-linear case they have a non-linear group structure. Algorithms to preserve the group structure are very complicated, especially in dynamics. Thus, eliminating the rotation field ab initio is a very attractive proposition.

During the last two decades, the technique of meshless interpolation of trial & test functions has been attracting a great attention. Meshless approximations, such as Moving Least Square(MLS), Reproducing Kernel (RK) and Partition of Unity Method (PU), possess intrinsic non-local properties. Unlike a typical finite element method, these non-local properties of meshfree approximations confer an arbitrary degree of smoothness on solutions and have been applied to various problems (Belytschko et al. 1994, Duarte et al. 1996, Babuska et al. 1997, Wendland 1999, Atluri et al. 1998, Atluri et al.1999, Atluri et al. 2000, Atluri et al. 2001, Gu and Liu 2001, Atluri & Shen 2002a,b). While an analysis of a class of meshless methods has appeared recently and provided a possibility to cope with high order elliptic problem conveniently, the real connection between them has not been made.

The purpose of the current paper is to report the details of a numerical approach, the Meshless Local Petrov-Galerkin (MLPG) method, to the Toupin-Mindlin formulation of strain gradient theories. The Meshless Local Petrov-Galerkin (MLPG) method was first introduced by Atluri et. al. in 1998, wherein the weak form of governing equations are based on local sub-domains, instead of whole domain in question. Subsequently the test function domains are also intentionally localized to sub-domains and, the space for test function may be completely different from that of trial function. MLPG is well-known as a truly meshfree method, in which two characteristics are guarantied: one is a non-element interpolation technique, and the other is a non-element approach for integrating the weak form. Most of the element-free methods are based on the non-element interpolation techniques, such as the Shepard interpolation technique (Shepard, 1968) and other approximations mentioned above, which do not need any elements for constructing the interpolation functions for the unknown variables. However, most of the meshless methods such as EFG, PKPM, and hp-clouds method, still require a global background mesh for numerical integration of the global weak form. Atluri and Shen in their pioneering work (2002a,b) have depicted the framework and application of MLPG method systematically, and successfully developed some fast and robust approaches. It should be noted that the MLPG concept is independent of a meshless interpolation technique, and it can be combined with any meshless interpolation technique, such as PUM, or PKPM. Furthermore, it can be shown that almost every other meshless method proposed in literature could be considered as a special case of MLPG.

In this paper, the main features of the MLPG are reviewed. The application of the MLPG to gradient theory is described in detail. To study the accuracy of the present method, convergence tests are carried out, and several 2-D problems of gradient theory have been analyzed. From these tests, the MLPG method is found to

give quite accurate results. The remarkable accuracy in these numerical simulations shows promising characteristics for solving general problems of materials whose constitutive laws involve strain-gradients.

2 Review of a linear elastic strain gradient theory

Toupin (1962) and Mindlin (1963, 1964) developed a theory of linear elasticity whereby the strain energy density w depends upon both the symmetric strain tensor $\varepsilon_{ij} \equiv \frac{1}{2}(u_{i,j} + u_{j,i})$and the second gradient of displacement, $\eta_{ijk} \equiv u_{k,ij}$. The corresponding compatibility equations are (Mindlin,1964):

$$\boldsymbol{\nabla} \times \boldsymbol{\varepsilon} \times \boldsymbol{\nabla} = \mathbf{0} \tag{1a}$$

$$\boldsymbol{\nabla} \times \boldsymbol{\eta} = 0 \tag{1b}$$

The strain energy function w is assumed to be a convex function, with respect to its arguments (ε, η) for each point $\mathbf{x}$ of a solid of volume V. The total energy Wstored in the solid is determined by the displacement field $\mathbf{u}(\mathbf{x})$ within V

$$W(\mathbf{u}) \equiv \int_V w(\varepsilon(\mathbf{u}), \eta(\mathbf{u}); \mathbf{x}) d\mathbf{x} \tag{1c}$$

with ε, η being derived from $\mathbf{u}$, as discussed above.

The energy variation of the solid due to an arbitrary variation of the displacement $\mathbf{u}$ is:

$$\delta W = \int_V (\sigma_{ij}\delta\varepsilon_{ij} + \tau_{ijk}\delta\eta_{ijk}) d\mathbf{x} \tag{2}$$

$$\sigma_{ij} \equiv \frac{\partial w}{\partial \varepsilon_{ij}};\ \tau_{ijk} \equiv \frac{\partial w}{\partial \eta_{ijk}}. \tag{3}$$

$$w = \frac{1}{2}\lambda\varepsilon_{ii}\varepsilon_{jj} + \mu\varepsilon_{ij}\varepsilon_{ij} + a_1\eta_{ijj}\eta_{ikk} + a_2\eta_{iik}\eta_{kjj} + a_3\eta_{iik}\eta_{jjk} + a_4\eta_{ijk}\eta_{ijk} + a_5\eta_{ijk}\eta_{jki} \tag{4a}$$

$$\sigma_{ij} = \frac{\partial w}{\partial \varepsilon_{ij}} = 2\mu\varepsilon_{ij} + \lambda\varepsilon_{kk}\delta_{ij} \tag{4b}$$

$$\tau_{ijk} = \frac{\partial w}{\partial \eta_{ijk}} = a_1(\eta_{ipp}\delta_{jk} + \eta_{jpp}\delta_{ik}) + a_2(\eta_{kpp}\delta_{ij} + \frac{1}{2}\eta_{ppi}\delta_{jk} + \frac{1}{2}\eta_{kkj}\delta_{ik}) + a_3(2\eta_{ppk}\delta_{ij}) + a_4(2\eta_{ijk}) + a_5(\eta_{jki} + \eta_{ikj}) \tag{4c}$$

Use of the divergence theorem transforms (3) into

$$\delta W = -\int_V [(\sigma_{jk,j} - \tau_{ijk,ij})\delta u_k] d\mathbf{x} + \int_S [(\sigma_{jk} - \tau_{ijk,i})n_j\delta u_k + \tau_{ijk}n_i\delta u_{k,j}] ds \tag{5}$$

where S is the surface bounding the volume V. Stationarity of the energy integral, with respect to the variations of the displacement field, provides the equilibrium relation

$$\sigma_{jk,j} - \tau_{ijk,ij} = 0 \tag{6}$$

To identify the required boundary conditions, we note that is not independent of on the surface S, because, if is known on S, so are the tangential gradients of at S. Therefore, six independent displacement boundary conditions are required for a correct formulation of the problem, e.g. prescribed values for $u_i,\ i = 1,2,3$ and their normal derivatives, at S.

In order to identify the independent traction boundary conditions, We separate the last integral of (5):

$$\tau_{ijk}n_i\delta u_{k,j} = \tau_{ijk}n_iD_j\delta u_k + \tau_{ijk}n_in_jD\delta u_k \tag{7}$$

by decomposing the gradient into a tangential gradient $D_j\delta u_k$ and a normal gradient $n_jD_\delta u_k$, viz.,

$$\delta u_{k,j} = D_j\delta u_k + n_jD_\delta u_k, \tag{8a}$$

where

$$D_j \equiv (\delta_{jp} - n_jn_p)\partial_p;\ \mathrm{D} \equiv n_p\partial_p \tag{8b}$$

and denotes the partial derivative with respect to x_p. The terms in (7) may be resolved, further, in more than one way. For the first term on the right hand side of (7), which contains the non-independent variation , we write (Mindlin, 1964)

$$\tau_{ijk}n_iD_j\delta u_k = D_j(\tau_{ijk}n_i\delta u_k) - n_iD_j\tau_{ijk}\delta u_k - (D_jn_i)\tau_{ijk}\delta u_k \tag{9}$$

The last two terms in (9) now contain the independent variation . For the preceding term, we note that , on the surface S,

$$D_j(\tau_{ijk}n_i\delta u_k) =$$

$$(D_l n_l)n_j n_i \tau_{ijk}\delta u_k + n_q e_{qpm}\partial_p(e_{mlj}n_l n_i \tau_{ijk}\delta u_k) \quad (10)$$

where is the alternating tensor. By Stokes's theorem, the integral, over a smooth surface, of the last term in (10) vanishes. If the surface has an edge C, formed by the intersection of two portions, S_1 and S_2, of S, Stokes's theorem gives

$$\int_S n_q e_{qpm}\partial_p(e_{mlj}n_l n_i \tau_{ijk}\delta u_k)dS = \oint_c [n_i m_j \tau_{ijk}]\delta u_k ds \quad (11)$$

where $m_j = e_{qpm}s_m n_l$ and the s_m are the components of the unit vector tangent to C. The bold face brackets **[ ]** in (11) indicate the enclosed quantity is the difference between the values on S_1 and S_2.

Now substitute (7), (9), (10) (11) into (5) and obtain the following final form of the principle of virtual work

$$\delta W = \int_S [t_k \delta u_k]ds + \int_S [R_k D\delta u_k]ds + \oint_c [n_i m_j \tau_{ijk}]\delta u_k ds, \quad (12)$$

where the surface traction on the surface S is

0A

$$t_k = n_i(\sigma_{ik} - \tau_{ijk,j}) + n_i n_j \tau_{ijk}(D_p n_p) - D_j(n_i \tau_{ijk}) \quad (13)$$

and the double stress traction R_k on S is

$$R_k = n_i n_j \tau_{ijk} \quad (14)$$

To summarize, the displacement field **u(x)** must satisfy three equilibrium equations given by the relation (6), and either the six traction boundary conditions given by (13) and (14), or the six displacement boundary conditions

$$u_i(\mathbf{x}) = u_i^0(\mathbf{x}),\ Du_i(\mathbf{x}) = v_i^0(\mathbf{x}),\ i = 1,2,3, \quad (15)$$

(or a mixture of them). A corollary of the above principle of virtual work is the stationarity principle

$$\int_V (\sigma_{ij}\delta\varepsilon_{ij} + \tau_{ijk}\delta\eta_{ijk})d\mathbf{x} = 0 \quad (16)$$

for any (ε, η) derived kinematically from a displacement field **u(x)** and for any (σ,τ) satisfying the equilibrium condition(5), and the zero traction conditions $t_k = R_k = 0$. It should be noted that, for convenience, we assume that the body double force (and also the body force) vanishes in this paper.

3 Review of Meshless Local Petrov-Galerkin (MLPG) method

The initial idea of meshless methods may date back to the smooth particle hydrodynamics (SPH) method for modeling astrophysical phenomena (Gingold and Monaghan, 1977). After Nayroles et al. published their work of Diffuse Element Method in 1992, the research about meshless methods turned to be very active. Since then, several meshless methods, such as Element Free Galerkin (EFG) by Belytschko et al. (1994), Reproducing Kernel Particle Method (RKPM) by Liu et al. (1996), the Partition of Unity Finite Element Method (PUFEM) by Babuska and Melenk (1997), hp-cloud method by Duarte and Oden 1996, Natural Element Method (NEM) by Sukumar et al. (1998) and Meshless Galerkin methods using Radial Basis Functions (RBF) by Wendland (1999), have also been reported in literature. The major differences in these meshless approaches focus on the techniques for interpolating the trial function. Although no mesh is required in these approximations for the trial and test functions for the unknowns, shadow elements(background meshes) are constructed for the integration of the weak-form, or of the 'energy'.

The meshless local Petrov-Galerkin (MLPG) method was first introduced by Atluri & Zhu (1998a, b) and Atluri et al. (1999) for solving linear and non-linear boundary value problems. The weak forms of governing PDE are based on local sub-domains, which may overlap each other in order to cover whole question domain. The spaces for trial and test functions may be different from each other(Atluri and Shen 2002a,b): the nodal trial function may correspond to any one of Moving Least Square(MLS), PU, Shepard function, or RBF types of

interpolations; and the test function may be totally different, which may correspond to any one of the above or even a Dirac delta function, the heaviside step function, the Gaussian weight function of MLS, a special form of the fundamental solution to the differential equation, or any other convenient function in the support domain, Ω_{te} (Fig.1), of the test function.

The Schematics of the MLPG method are shown in Fig. 1, where the support domain of weight function at any node ***I*** is usually taken as a circle in 2-D cases with its radius r_I. The interpolation of trial function at any point **x** should involve all the nodes whose support domains cover this point. Also the node based test domain (also taken as a circle in 2-D for convenience) with radius r_J could have a different size from that of shape function. It should be noted that, in Fig.1 the domain of support of the test function Ω_{te}^{I} is synonymous with the node-based sub-domain.

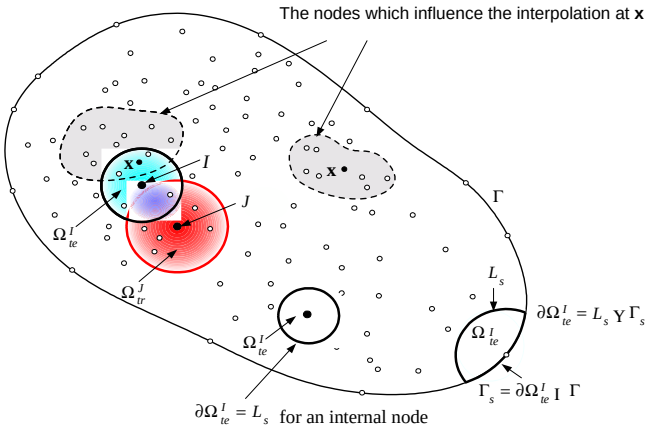

Figure 3.1: Schematics of the MLPG method

There are no more background meshes needed for purpose of the integration of the weak form in the MLPG method, i.e., all pertinent integrals can be easily evaluated over well-shaped sub-domains, and on their boundaries. For instance, in 2-D cases, we may define all the sub-domains that are based on inner nodes (i.e. inside the domain) as circular domains without intersection with global boundaries. Every sub-domain based on the boundary node is a part of circle. Then integration of sub-domain based weak form may be simply evaluated on the circles (or part of a circle). Fig 3.2 shows the intersections between supports of nodal shape functions and some specific inner sub-domain(i.e. test domain). Also one may define inner sub-domains that intersect global boundaries in more general. There are several approaches introduced by Atluri et al.(2002a, b) to handle those more complicate cases.

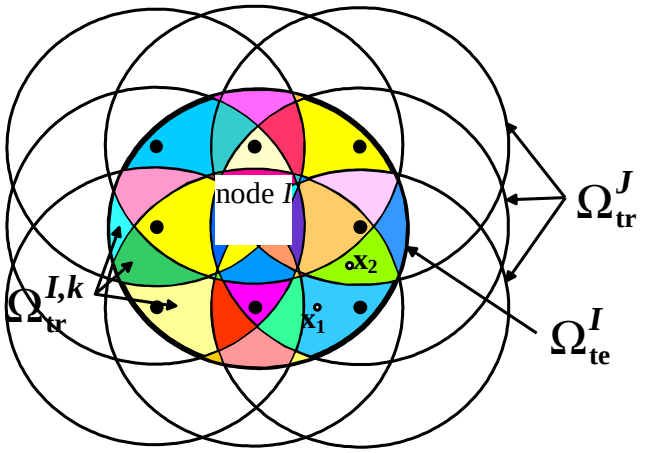

Figure 3.2: The nodal shape function has a different form in each small region $\Omega_{tr}^{I,k}$, which is the intersection of Ω_{te}^{I} and Ω_{tr}^{J}.

4 MLGP Method for Materials with Strain-Gradient Effects

4.1 Weak forms based on sub-domains

Now we proceed to apply MLPG method to solids involving gradient theories. Re-write the governing equation (6) in the domain Ω bounded by the boundary Γ as follows,

$$\sigma_{jk,j} - \tau_{ijk,ij} = 0 \quad , \tag{17}$$

with boundary conditions :

$$u_i(\mathbf{x}) = u_i^0(\mathbf{x}), Du_i(\mathbf{x}) = v_i^0(\mathbf{x}), i = 1,2,3, \text{ on } \mathbf{\Gamma}_u \tag{18a}$$

or

$$t_i(\mathbf{x}) = t_i^0(\mathbf{x}), R_i(\mathbf{x}) = R_i^0(\mathbf{x}), i = 1,2,3 \text{ on } \mathbf{\Gamma}_t \tag{18b}$$

or a mixture of them, where , are the prescribed displacements and their normal derivatives on boundary, and , are the surface traction and the double stress traction. u_k denotes a displacement field satisfying (17) with corresponding constitutive relationships. The constitutive equations and strain-displacement relationship are defined in preceding sections.

Meshless methods based on global Galerkin formulation usually begin with the global weak form of governing equation over the entire domain Ω. However in the present local Petrov-Galerkin formulation, we start from a weak form over a local sub-domain Ω_s, and use the MLS approximation to develop a truly meshless method, where the local sub-domain Ω_s is located entirely inside the global domain Ω. The local sub-domian Ω_s is conveniently taken to be a sphere (in 3-D, or a circle in 2-D) centered at a point $\mathbf{x}$ in domain. A generalized local weak form of the differential equation (17) and the boundary conditions (4.2a,b), over a local sub-domain Ω_s, can be written as:

$$\int_{\Omega_s}(\sigma_{jk,j}-\tau_{ijk,ij})\rho_k d\mathbf{x}-\alpha\int_{\Gamma s_u}(u_k-u_k^0)\rho_k ds$$
$$-\beta\int_{\Gamma} s_{Du}(v_k-v_k^0)\rho_k ds=0 \tag{19}$$

with local boundary conditions

$$u_k(\mathbf{x})=u_k^0(\mathbf{x}), Du_k(\mathbf{x})\equiv v_k=v_k^0(\mathbf{x}), k=1,2,3, \text{ on } \mathbf{\Omega}s \tag{20a}$$

or

$$t_k(\mathbf{x})=t_k^0(\mathbf{x}), R_k(\mathbf{x})=R_k^0(\mathbf{x}), k=1,2,3 \text{ on } \mathbf{\Omega}s \tag{20b}$$

or mixture of them, where , ρ_k are trial and test function, respectively, and $v_k=Du_k=u_{k,i}n_i$,. Γs is a part of $\partial\Omega_s$, over which the boundary conditions are specified. In general, $\partial\Omega_s=\Gamma_s\cup L_s$, with Γ_s being a part of the local boundary located on the global boundary, and let L_s being the other part of the local boundary over which no boundary condition is specified, i.e., $\Gamma_s=\partial\Omega_s\cap\Gamma$, (see Fig. 1). For a sub-domain located entirely inside the global domain, there is no intersection between $\partial\Omega_s$ and Γ, L_s= $\partial\Omega_s$. Then Γs_u and Γs_{Du} denote boundary conditions of displacement and normal gradient of displacement, respectively. α , β are two constants in penalty functions for handling essential boundary conditions. As long as the sub-domains cover whole question domains, the weak forms based on local sub-domains are equivalent with weak form defined on whole domain(Atluri and Shen, 2002a, b).

From equations in the preceding sections, it is straightforward to obtain following weak form,

$$\int_{\partial\Omega_s}t_k\rho_k ds+\int_{\partial\Omega_s}R_kD\rho_k ds$$
$$+\int_{\partial\Omega_s}n_q e_{qpm}\partial_p(e_{mlj}n_l n_i\tau_{ijk}\rho_k)dS$$
$$-\int_{\Omega_s}(\sigma_{jk}\rho_{k,j}+\tau_{ijk}\rho_{k,ij})d\mathbf{x}-\alpha\int_{\Gamma s_u}(u_k-u_k^0)\rho_k ds$$
$$-\beta\int_{\Gamma s_{Du}}(v_k-v_k^0)\rho_k ds=0 \tag{21}$$

According to (11), the third term in left hand side vanishes if the sub-domain does not intersect with global boundary Γ, i.e. $\Omega_s\cup\Gamma_s$ =Ø. In two-dimensional cases the integral over global boundary Γ may be replaced by

$$\sum_{\gamma}[n_i m_j\tau_{ijk}]_{\gamma}\rho_k \tag{22}$$

where the sum over γ refers to any corners that may exist on the global bounding curve of the two-dimensional body. It should be noted that, in all the coming examples, (22) will vanish identically on boundaries, so that for convenience we will not repeat this term in the final weak form and consequent procedures in calculations. Then we may re-arrange (21) into

$$\alpha\int_{\Gamma s_u}u_k\rho_k ds+\beta\int_{\Gamma s_{Du}}v_k\rho_k ds$$
$$+\int_{\Omega_s}(\sigma_{jk}\rho_{k,j}+\tau_{ijk}\rho_{k,ij})d\mathbf{x}-\int_{\Gamma s_u+Ls}t_k\rho_k ds$$
$$-\int_{\Gamma s_{Du}+Ls}R_kD\rho_k ds=\alpha\int_{\Gamma s_u}u_k^0\rho_k ds+\beta\int_{\Gamma s_{Du}}v_k^0\rho_k ds$$
$$+\int_{\Gamma s_t}t_k^0\rho_k ds+\int_{\Gamma s_R}R_k^0D\rho_k ds \tag{23}$$

wherein Γs_t and Γs_R denote boundary conditions of surface traction and the double stress traction, respectively. All the natural boundary conditions have been imposed in (23). In MLPG method (Atluri and Shen 2002a,b), test functions ρ_k are treated as functions that are different from the trial functions. For convenience, we may

localize test functions onto sub-domain, such that ρ_k and $D\rho_k$ vanish on the boundary L_s. Then (23) could be simplified further to be

$$\alpha\int_{\Gamma s_u} u_k\rho_k ds+\beta\int_{\Gamma s_{Du}} v_k\rho_k ds+\int_{\Omega_s}(\sigma_{jk}\rho_{k,j}+\tau_{ijk}\rho_{k,ij})d\mathbf{x}$$
$$-\int_{\Gamma s_u} t_k\rho_k ds-\int_{\Gamma s_{Du}} R_k D\rho_k ds=\alpha\int_{\Gamma s_u} u_k^0\rho_k ds$$
$$+\beta\int_{\Gamma s_{Du}} v_k^0\rho_k ds+\int_{\Gamma s_t} t_k^0\rho_k ds+\int_{\Gamma s_R} R_k^0 D\rho_k ds \qquad (24)$$

Recalling the definitions of τ_{ijk}, η_{ijk}, and in preceding sections, due to the presence of derivative of higher order stress in the surface traction (see equation 2.12), we must introduce at least C^2-continuity interpolation scheme for the trial function, in order to guarantee the convergence of numerical solution.

4.2 Meshfree interpolation for trial function and test function

In general, meshless methods use a local interpolation or an approximation to represent the trial function , using the values (or the fictitious values) of the unknown variable at some randomly located nodes in the local vicinity. A variety of local interpolation schemes that interpolate the data at randomly scattered points(without the need for a mesh) in two or more independent variables are currently available(Atluri and Shen, 2002a,b):

i. Shepard Functions (Shpard, 1968), which have a consistency of zeroth order only;

ii. Moving Least Squares interpolation (MLS) (Lancaster & Salkauskas, 1981; Nayroles, Touzot & Villon, 1992), which generalizes Shepard's approach, implicitly, to the case of shape functions of high order consistency;

iii. Partition of Unity Methods (Bauska & Melenk, 1997), which generalizes Shepard's approach, explicitly, to higher orders of consistency;

iv. Reproducing Kernel Particle Methods (Liu, Chen, Uras & Chang, 1996), which are identical to the MLS approach, if the kernel is identical to the weight functin of a MLS approximation, and is rendered to be higher order consistent by same basis;

v. Radial Basis Functions (Wendland, 1995), which use random points in the domain, and generate the required trial & test functions.

The moving least-square method, which is adopted in this paper, is generally considered to be one of the best schemes to interpolate data with a reasonable accuracy. Basically the MLS interpolation does not pass through the nodal data, as shown in Fig. 4.1. Here we give a brief summary of the MLS approximation. For details of the MLS approximation, see Belytschko et al. (1994) and Atluri et al. (1999).

Consider a domain in question with control points for boundaries (i.e. nodes on boundaries) and some scattered nodes inside, where every node has its nodal value (fictitious) and influence radius(radius for local weight function). Now for the distribution of trial function at any point $\mathbf{x}$ and its neighborhood located in the problem domain Ω, $u^h(\mathbf{x})$ may be defined by

$$u^h(\mathbf{x})=\mathbf{p}^T(\mathbf{x})\,\mathbf{a}(\mathbf{x})\;\forall\mathbf{x}\in\Omega_{\mathbf{x}} \qquad (25a)$$

where $\mathbf{p}^T(\mathbf{x})=[p_1(\mathbf{x}),\ p_2(\mathbf{x}),\ \ldots,p_m(\mathbf{x})]$ is a complete monomial basis of order m, and $\mathbf{a}(\mathbf{x})$ is a vector containing coefficients $a_j(\mathbf{x})$, j=1, 2, …,m which are functions of the space co-ordinates $\mathbf{x}=[x_1,x_2,x_3]^T$. The commonly used bases in 2-D or 3-D are the linear basis, due to their simplicity. In Zhu et al. (1998) and Atluri et al. (1998), both linear and quadratic basis are used, and the results show that both bases possess high accuracy. In the present high order elliptic problem, we will begin with the quadratic basis

$$\mathbf{p}^T(\mathbf{x})=[1,x_1,x_2,x_1^2,x_1x_2,x_2^2] \qquad (25b)$$

for 2-D, wherein m=6.

The coefficient vector $\mathbf{a}(\mathbf{x})$ is determined by minimizing a weighted discrete L_2 norm, which can be defined as

$$J(\mathbf{x})=\sum_{I=1}^{N} w_I(\mathbf{x})\left[\mathbf{p}^T(\mathbf{x}_I)\,\mathbf{a}(\mathbf{x})-\hat{u}^I\right]^2 \qquad (26)$$

where $w_I(\mathbf{x})$, is a weight function associated with the node I, with $w_I(\mathbf{x})>0$ for all $\mathbf{x}$ in the support of $w_I(\mathbf{x})$, $\mathbf{x}_I$ denotes the value of $\mathbf{x}$ at node I, N is the number of nodes in Ω_x for which the weight functions $w_I(\mathbf{x})>0$.

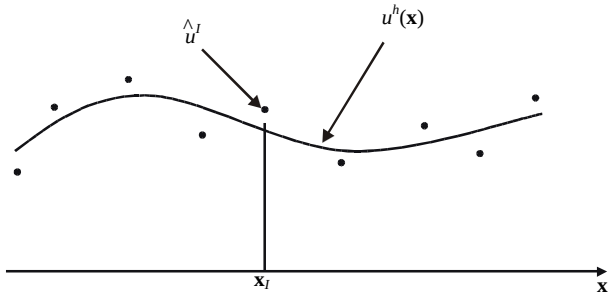

Figure 4.1: The distinction between u^I and $\hat{u}^I$.

Here it should be noted that $\hat{u}^I$, I=1, 2,..., N, in equation (26), are the fictitious nodal values, and not the actual nodal values of the unknown trial function $u^h(\mathbf{x})$, in general (see Fig. 4.1 for a simple one-dimensional case for the distinction between u^I and $\hat{u}^I$).

Solving for $\mathbf{a}(\mathbf{x})$ by minimizing J in equation (26), and substituting it into equation (4.9), give a relation which may be written in the form of an interpolation function similar to that used in the FEM, as

$$u^h(\mathbf{x}) = \sum_{I=1}^{N} \phi^I(\mathbf{x})\,\hat{u}^I, \tag{27}$$

where

$$\phi^I(\mathbf{x}) = \sum_{j=1}^{m} p_j(\mathbf{x}) \left[\mathbf{A}^{-1}(\mathbf{x})\mathbf{B}(\mathbf{x})\right]_{jI} \tag{28}$$

with the matrix $\mathbf{A}(\mathbf{x})$ and $\mathbf{B}(\mathbf{x})$ being defined by:

$$\mathbf{A}(\mathbf{x}) = \sum_{I=1}^{N} w_I(\mathbf{x})\,\mathbf{p}(\mathbf{x}_I)\,\mathbf{p}^T(\mathbf{x}_I) \tag{29}$$

$$\mathbf{B}(\mathbf{x}) = [w_1(\mathbf{x})\,\mathbf{p}(\mathbf{x}_1),\ w_2(\mathbf{x})\,\mathbf{p}(\mathbf{x}_2),\ \cdots,\ w_N(\mathbf{x})\,\mathbf{p}(\mathbf{x}_N)] \tag{30}$$

The partial derivatives of $\phi^I(\mathbf{x})$ are obtained as

$$\phi^I_{,k} = \sum_{j=1}^{m} \left[p_{j,k}\left(\mathbf{A}^{-1}\mathbf{B}\right)_{jI} + p_j\left(\mathbf{A}^{-1}\mathbf{B}_{,k} + \mathbf{A}^{-1}_{,k}\mathbf{B}\right)_{jI}\right] \tag{31}$$

in which

$$\mathbf{B}_{,k}(\mathbf{x}) = \left[w_{1_{,k}}(\mathbf{x})\,\mathbf{p}(\mathbf{x}_1), w_{2_{,k}}(\mathbf{x})\,\mathbf{p}(\mathbf{x}_2),\right.$$
$$\left.\ldots, w_{N_{,k}}(\mathbf{x})\,\mathbf{p}(\mathbf{x}_N)\right] \tag{32}$$

and $\mathbf{A}^{-1}_{,k} = \left(\mathbf{A}^{-1}\right)_{,k}$ represents the derivative of the inverse of A with respect to x^k, which is given by

$$\mathbf{A}^{-1}_{,k} = -\mathbf{A}^{-1}\mathbf{A}_{,k}\mathbf{A}^{-1} \tag{33}$$

with

$$\mathbf{A}_{,k}(\mathbf{x}) = \sum_{I=1}^{N} w_{I_{,k}}(\mathbf{x})\,\mathbf{p}(\mathbf{x}_I)\,\mathbf{p}^T(\mathbf{x}_I) \tag{34}$$

The second and third partial derivatives of $\phi^I(\mathbf{x})$ may be obtained in similar way:

$$\begin{aligned}\phi^I_{,kl} = \sum_{j=1}^{m} \Big[& p_{j,kl}\left(\mathbf{A}^{-1}\mathbf{B}\right)_{jI} + p_{j,k}\left(\mathbf{A}^{-1}_{,l}\mathbf{B} + \mathbf{A}^{-1}\mathbf{B}_{,l}\right)_{jI} \\ & + p_{j,l}\left(\mathbf{A}^{-1}\mathbf{B}_{,k} + \mathbf{A}^{-1}_{,k}\mathbf{B}\right)_{jI} \\ & + p_j\left(\mathbf{A}^{-1}_{,l}\mathbf{B}_{,k} + \mathbf{A}^{-1}\mathbf{B}_{,kl} + \mathbf{A}^{-1}_{,kl}\mathbf{B} + \mathbf{A}^{-1}_{,k}\mathbf{B}_{,l}\right)_{jI}\Big]\end{aligned} \tag{35}$$

$$\begin{aligned}\phi^I_{,kli} = \sum_{j=1}^{m} \Big[& p_{j,kli}\left(\mathbf{A}^{-1}\mathbf{B}\right)_{jI} + p_{j,kl}\left(\mathbf{A}^{-1}_{,i}\mathbf{B} + \mathbf{A}^{-1}\mathbf{B}_{,i}\right)_{jI} + \\ & p_{j,ki}\left(\mathbf{A}^{-1}_{,l}\mathbf{B} + \mathbf{A}^{-1}\mathbf{B}_{,l}\right)_{jI} + \\ & p_{j,k}\left(\mathbf{A}^{-1}_{,li}\mathbf{B} + \mathbf{A}^{-1}_{,l}\mathbf{B}_{,i} + \mathbf{A}^{-1}_{,i}\mathbf{B}_{,l} + \mathbf{A}^{-1}\mathbf{B}_{,li}\right)_{jI} + \\ & p_{j,li}\left(\mathbf{A}^{-1}\mathbf{B}_{,k} + \mathbf{A}^{-1}_{,k}\mathbf{B}\right)_{jI} + \\ & p_{j,l}\left(\mathbf{A}^{-1}_{,i}\mathbf{B}_{,k} + \mathbf{A}^{-1}\mathbf{B}_{,ki} + \mathbf{A}^{-1}_{,ki}\mathbf{B} + \mathbf{A}^{-1}_{,k}\mathbf{B}_{,i}\right)_{jI} + \\ & p_{j,i}\left(\mathbf{A}^{-1}_{,l}\mathbf{B}_{,k} + \mathbf{A}^{-1}\mathbf{B}_{,kl} + \mathbf{A}^{-1}_{,kl}\mathbf{B} + \mathbf{A}^{-1}_{,k}\mathbf{B}_{,l}\right)_{jI} + \\ & p_j\left(\begin{array}{l}\mathbf{A}^{-1}_{,li}\mathbf{B}_{,k} + \mathbf{A}^{-1}_{,l}\mathbf{B}_{,ki} + \mathbf{A}^{-1}_{,i}\mathbf{B}_{,kl} + \mathbf{A}^{-1}\mathbf{B}_{,kli} + \\ \mathbf{A}^{-1}_{,kli}\mathbf{B} + \mathbf{A}^{-1}_{,kl}\mathbf{B}_{,i} + \mathbf{A}^{-1}_{,ki}\mathbf{B}_{,l} + \mathbf{A}^{-1}_{,k}\mathbf{B}_{,li}\end{array}\right)_{jI}\Big]\end{aligned} \tag{36}$$

with

$$\begin{aligned}\mathbf{A}^{-1}_{,kl} = & \mathbf{A}^{-1}\mathbf{A}_{,l}\mathbf{A}^{-1}\mathbf{A}_{,k}\mathbf{A}^{-1} - \mathbf{A}^{-1}\mathbf{A}_{,kl}\mathbf{A}^{-1} \\ & + \mathbf{A}^{-1}\mathbf{A}_{,k}\mathbf{A}^{-1}\mathbf{A}_{,l}\mathbf{A}^{-1}\end{aligned} \tag{37}$$

$$\mathbf{A}^{-1}_{,kli} = (\mathbf{A}^{-1}_{,kl})_{,i} =$$

$$-(\mathbf{A}^{-1}_{,l}\mathbf{A}_{,k}\mathbf{A}^{-1} - \mathbf{A}^{-1}\mathbf{A}_{,kl}\mathbf{A}^{-1} + \mathbf{A}^{-1}\mathbf{A}_{,k}\mathbf{A}^{-1}_{,l})_{,i} =$$

$$-(\mathbf{A}^{-1}_{,li}\mathbf{A}_{,k}\mathbf{A}^{-1} + \mathbf{A}^{-1}_{,l}\mathbf{A}_{,ki}\mathbf{A}^{-1} + \mathbf{A}^{-1}_{,l}\mathbf{A}_{,k}\mathbf{A}^{-1}_{,i}$$

$$-\mathbf{A}^{-1}_{,i}\mathbf{A}_{,kl}\mathbf{A}^{-1} - \mathbf{A}^{-1}\mathbf{A}_{,kli}\mathbf{A}^{-1} - \mathbf{A}^{-1}\mathbf{A}_{,kl}\mathbf{A}^{-1}_{,i}$$

$$+\mathbf{A}^{-1}_{,i}\mathbf{A}_{,k}\mathbf{A}^{-1}_{,l} + \mathbf{A}^{-1}\mathbf{A}_{,ki}\mathbf{A}^{-1}_{,l} + \mathbf{A}^{-1}\mathbf{A}_{,k}\mathbf{A}^{-1}_{,li}) \tag{38}$$

$$\mathbf{B}_{,kl}(\mathbf{x}) = \left[w_{1_{,kl}}(\mathbf{x})\mathbf{p}(\mathbf{x}_1), w_{2_{,kl}}(\mathbf{x})\mathbf{p}(\mathbf{x}_2),\right.$$

$$\left.\cdots, w_{N_{,kl}}(\mathbf{x})\mathbf{p}(\mathbf{x}_N)\right] \tag{39}$$

$$\mathbf{B}_{,kli}(\mathbf{x}) = \left[w_{1_{,kli}}(\mathbf{x})\mathbf{p}(\mathbf{x}_1), w_{,kli}(\mathbf{x})\mathbf{p}(\mathbf{x}_2),\right.$$

$$\left.\ldots, w_{N_{,kli}}(\mathbf{x})\mathbf{p}(\mathbf{x}_N)\right] \tag{40}$$

The MLS approximation is well defined, only when the matrix in Eq. (29) is non-singular. $\phi^I(\mathbf{x})$ is usually called the shape function of the MLS approximation, corresponding to the nodal point $\mathbf{x}_I$. FromEqs. (28) and (30), it may be seen that $\phi^I(\mathbf{x})$=0 when $w_I(\mathbf{x})$=0. The fact that $\phi^I(\mathbf{x})$ vanishes, as defined, for $\mathbf{x}$ not in the support of nodal point, $\mathbf{x}_I$ preserves the local character of the moving least squares approximation. The nodal shape function is complete up to the highest order of the basis. The smoothness of the nodal shape function is determined by that of the basis and weight function.

The choice of the weight function is more or less arbitrary, as long as the weight function is positive and continuous and satisfies the continuity requirement in weak form. Since C^2 continuity is needed in current computation, (see similar approach by Long and Atluri, 2002) the weight function corresponding to node I may be written as

$$w_I(\mathbf{x}) = \begin{cases} (1-(d_I/r_I)^2)^3, & 0 \le d_I \le r_I \\ 0, & d_I \ge r_I \end{cases} \tag{41a}$$

where $d_I = |\mathbf{x}-\mathbf{x}_I|$ is the distance from node $\mathbf{x}_I$ to point $\mathbf{x}$ and r_I is the size of the support for the weight function w_I (and thus determines the influence domain of node $\mathbf{x}_I$). The size of support, r_I of the weight function w_I associated with node I should be chosen such that r_I should be large enough to have sufficient number of nodes covered in the domain of definition of every sample point ($n \ge m$), in order to ensure the regularity of $\mathbf{A}$. Usually, we have to guarantee all the nodes covered in the domain of definition of every sample point can not be on a single line if linear interpolation space is applied; all of these nodes can not be on two lines if quadratic space is applied. A very small r_I may result in a relatively large numerical error while using the Gauss numerical quadrature to calculate the entires in the system stiffness matrix. On the other hand, r_I should also be small enough to maintain the local character of the MLS approximation. It can be easily seen that the weight function (4.25) possesses C^2 continuity. Thus as discussed in detail in Atluri and Shen (2002a,b), the MLS, and the corresponding trial functions are C^2 continuous over the entire domain.

The consistency condition, namely the ability of the MLS interpolation (27) to exactly represent the jth [j=1,2,....m] component of monomials in (4.9b), implies that in general

$$\sum_{I=1}^{N} \phi_I(\mathbf{x}) x^l_{Ii} = x^l_i \ \forall \mathbf{x} \in \Omega, \forall l \le k \tag{41b}$$

where $k$is the highest order in the base. In fact, the linear basis assures that the MLS approximation has the linear completeness. Thus, it can reproduce any smooth function and its first derivative with arbitrary accuracy, as the approximation is refined. Quadratic or higher order base has similar characteristics.

A generalization of the MLS interpolation scheme using the data for the derivative of a function, in addition to the value of the function itself, at a finite number of nodes, can be found in Atluri et al (1999).

The choice of test function is somewhat arbitrary in the MLPG method. The various features of the MLPG have been illustrated (Atluri and Shen 2002a,b), by solving linear Poisson's equation with use of different kinds

of the test functions, including MLS weight function (MLPG1), the collocation Dirac's Delta function (MLPG2), discrete least squares (i.e. error function, MLPG3), modified fundamental solution to the PDEs(MLPG4), Heaviside step function(MLPG5) and also nodal shape functions (i.e local Galerkin method, MLPG6). In MLPG6, the integrand is far more complex than in the five other MLPGs, due to the fact that the test function comes from the same space of the trial function. Furthermore, the partition method must be used to obtain a convergent result (Atluri,et al 1999); similar situation exists in MLPG3, where, additionally, a trial function with higher order continuity requirement is needed; MLPG4 would be very attractive as long as the fundamental solution of PDE is available, although the integration with the singularity has to be handled; the concept of MLPG2 is very similar with that of the Collocation Method, where the numerical accuracy is found to be sensitive to the distribution and density of the nodes; the main purpose of MLPG1 is to avoid evaluating the integration on the local boundary, because the MLS weight function always vanishes over the local boundary (in equation 4.7, we have to look for a test function such that its normal gradient over the local boundary also vanishes); by taking constant as the test function over every sub-domain, domain integral is altogether avoided in the MLPG5, which is widely considered as a robust, fast and also accurate approach, when solving 2^{nd} order BVPs.

However, in current problem (from the local weak form (23)), the feature of MLPG5 can not show its advantages (usually taken to eliminate the need of domain integration, but can not avoid all the integration over local boundary): if we consider a constant (i.e. Heaviside step function) as the test function over every sub-domain, the last term of right hand side of (23) vanishes (also does the last term of left hand side), so that the double stress traction can not be imposed. In other hand, selecting other simple function, such as linear function etc., to be a test function in each local test domain, may eliminate one of the two domain integrals in (23), but incurs all the local boundary integration inevitably.

Then we resort to the concept of MLPG1. It is seen that the local weak form over Ωs involves both the first derivative as well as the second derivative of ρ_k in domain integrand. Thus the test function for every subdomain at least needs C^1 continuity over the local subdomain. In order to eliminate the integral over the local boundary, we consider a localized spline weight function to be the test function, which is defined as:

$$\rho_I(\mathbf{x})=\begin{cases} 1-6\left(\frac{d_I}{R_I}\right)^2+8\left(\frac{d_I}{R_I}\right)^3-3\left(\frac{d_I}{R_I}\right)^4, & 0\le d_I\le R_I \\ 0, & d_I\ge R_I \end{cases} \tag{42}$$

such that ρ_k and $D\rho_k$ vanish on the boundary L_s required to obtain (24), where R_I is the size of the support for the weight function, which is usually much smaller than size of support domain of shape function. It should be noted that the test functions satisfying these requirements are not unique and could have other forms, such as $\left(1-(d_I/R_I)^2\right)^2$, or even the current MLS weight function $\left(1-(d_I/R_I)^2\right)^3$, or the proper Gaussian weight functions, etc. All of these choices come from the framework of MLPG1 and it is found that there is no obvious difference among the rates of convergence when applying any of weight functions above as test function (Atluri and Shen 2002a, b). And that is confirmed again in current calculations.

4.3 Discretization of the weak form with plane strain assumption

The plane strain assumption is taken in all of examples in this paper. In general , the displacement fields are

$$\begin{aligned} &u_i = u_i(x_1,x_2)\ i=1,2 \\ &u_3 = 0\ , \end{aligned} \tag{43}$$

strains and strain gradients are

$$\begin{aligned} &\varepsilon_{ij}=\tfrac{1}{2}(u_{i,j}+u_{j,i})\ i=1,2;\ j=1,2 \\ &\varepsilon_{3m}=0\ m=1,2,3 \\ &\eta_{ij\gamma}=u_{\gamma,ij}\ \gamma=1,2 \\ &\eta_{ij3}=0 \\ &\eta_{3j\gamma}=\eta_{j3\gamma}=0\ , \end{aligned} \tag{44}$$

and the corresponding conventional and high order stresses are

$$
\begin{aligned}
&\sigma_{ij} = \lambda\varepsilon_{pp}\delta_{ij} + 2\mu\varepsilon_{ij} \\
&\sigma_{33} = \nu\sigma_{pp} \\
&\sigma_{3m} = 0 \\
&\tau_{ijk} = a_1(\eta_{ipp}\delta_{jk} + \eta_{jpp}\delta_{ik}) \\
&\quad + a_2(\eta_{kpp}\delta_{ij} + \tfrac{1}{2}\eta_{ppi}\delta_{jk} + \tfrac{1}{2}\eta_{kkj}\delta_{ik}) \\
&\quad + a_3(2\eta_{ppk}\delta_{ij}) + a_4(2\eta_{ijk}) + a_5(\eta_{jki} + \eta_{ikj}) \\
&i, j, k, p = 1, 2 \\
&m = 1, 2, 3
\end{aligned} \tag{45}
$$

The weak form (24) that is based on any sub-domain then could be written as

$$
\begin{aligned}
&\sum_{i=1}^{N} \Bigg\{ \int_{\Omega_s} ([B_{\rho_\sigma}][D_\sigma][B_{\phi_\sigma}] + [B_{\rho_\tau}][D_\tau][B_{\phi_\tau}])\{\hat{u}^i\} d\mathbf{x} \\
&- \int_{\Gamma s_u} [S_u] \\
&\begin{pmatrix} [n_i\rho^J]_\sigma[D_\sigma][B_{\phi_\sigma}] - [n_i\rho^J]_\tau[D_{\tau'}][B_{\phi'_\tau}] \\ +(D_p n_p)\rho^J[n_i n_j][D_\tau][B_{\phi_\tau}] - \rho^J[D_j n_i][D_\tau][B_{\phi_\tau}] \\ -\rho^J[n_i D_j][D_{\tau'}][B_{\phi'_\tau}] \end{pmatrix} \{\hat{u}^i\} ds \\
&- \int_{\Gamma s_{Du}} (D\rho^J)[S_{Du}][n_i n_j][D_\tau][B_{\phi_\tau}]\{\hat{u}^i\} ds \\
&+ \int_{\Gamma s_u} \alpha\rho^J[S_u][\phi_u]\{\hat{u}^i\} ds \\
&+ \int_{\Gamma s_{Du}} \beta\rho^J[S_{Du}][\phi_{Du}]\{\hat{u}^i\} ds \Bigg\} \\
&= \int_{\Gamma s_u} \alpha\rho^J \{\mathbf{u}^0\} ds + \int_{\Gamma s_{Du}} \beta\rho^J \{D\mathbf{u}^0\} ds \\
&+ \int_{\Gamma s_t} \rho^J \{\mathbf{t}^0\} ds + \int_{\Gamma s_R} \rho^J \{\mathbf{R}^0\} ds
\end{aligned} \tag{46}
$$

where ρ^J denotes test function (localized spline weight function) on node J based sub-domain. 'i' denotes node number and N is the total number of nodes, and

$$
[B_{\rho_\sigma}] = \begin{bmatrix} \rho_{,1} & 0 & \rho_{,2} \\ 0 & \rho_{,2} & \rho_{,1} \end{bmatrix} \quad ; \quad [B_{\phi_\sigma}] = \begin{bmatrix} \phi_{,1} & 0 \\ 0 & \phi_{,2} \\ \phi_{,2} & \phi_{,1} \end{bmatrix}; \tag{47a}
$$

$$
[B_{\rho_\tau}] = \begin{bmatrix} \rho_{,11} & \rho_{,22} & 2\rho_{,12} & 0 & 0 & 0 \\ 0 & 0 & 0 & \rho_{,11} & \rho_{,22} & 2\rho_{,12} \end{bmatrix}; \tag{47b}
$$

$$
[B_{\phi_\tau}] = \begin{bmatrix} \phi_{,11} & \phi_{,22} & \phi_{,12} & 0 & 0 & 0 \\ 0 & 0 & 0 & \phi_{,11} & \phi_{,22} & \phi_{,12} \end{bmatrix}^T; \tag{47c}
$$

$$
\{\hat{u}^i\} = \{\hat{u}^i_1 \ \hat{u}^i_2\}^T; \quad [n_i\rho^J]_\sigma = \rho^J \begin{bmatrix} n_1 & 0 & n_2 \\ 0 & n_2 & n_1 \end{bmatrix}; \tag{47d}
$$

$$
[n_i\rho^J]_\tau = \rho^J \begin{bmatrix} n_1 & 0 & n_2 & 0 & 0 & 0 & 0 & n_2 & n_1 & 0 & 0 & 0 \\ 0 & 0 & 0 & n_1 & 0 & n_2 & 0 & 0 & 0 & 0 & n_2 & n_1 \end{bmatrix}; \tag{47e}
$$

$$
[B_{\phi'_\tau}] = \begin{bmatrix} \phi_{,111} & \phi_{,122} & \phi_{,112} & 0 & 0 & 0 \\ 0 & 0 & 0 & \phi_{,111} & \phi_{,122} & \phi_{,112} \\ \phi_{,112} & \phi_{,222} & \phi_{,122} & 0 & 0 & 0 \\ 0 & 0 & 0 & \phi_{,112} & \phi_{,222} & \phi_{,122} \end{bmatrix}^T; \tag{47f}
$$

$$
[n_i n_j] = \begin{bmatrix} n_1 n_1 & n_2 n_2 & 2n_1 n_2 & 0 & 0 & 0 \\ 0 & 0 & 0 n_1 n_1 & n_2 n_2 & 2n_1 n_2 & \end{bmatrix}; \tag{47g}
$$

$[D_j n_i]$is a matrix with dimension 2x6, where

$$
\begin{aligned}
&[D_j n_i]_{11} = (1 + n_1^2) n_{1,1} + n_1 n_2 n_{1,2} \\
&[D_j n_i]_{12} = (1 + n_2^2) n_{2,2} + n_1 n_2 n_{2,1} \\
&[D_j n_i]_{13} = (1 + n_1^2) n_{2,1} + (1 + n_2^2) n_{1,2} + n_1 n_2 (n_{1,1} + n_{2,2}) \\
&[D_j n_i]_{24} = [D_j n_i]_{11} \\
&[D_j n_i]_{25} = [D_j n_i]_{12} \\
&[D_j n_i]_{26} = [D_j n_i]_{13}
\end{aligned} \tag{47h}
$$

and other components vanish. $[n_i D_j]$ is a matrix with dimension 2x12, where

$$[n_i D_j] = \begin{bmatrix} n_1 & 0 & n_2 & 0 & 0 & 0 & 0 & n_2 & n_1 & 0 & 0 & 0 \\ 0 & 0 & 0 & n_1 & 0 & n_2 & 0 & 0 & 0 & 0 & n_2 & n_1 \end{bmatrix} - \begin{bmatrix} n_1^3 & n_1 n_2^2 & 2n_1^2 n_2 & 0 & 0 & 0 \\ 0 & 0 & 0 & n_1^3 & n_1 n_2^2 & 2n_1^2 n_2 \\ n_1^2 n_2 & n_2^3 & 2n_1 n_2^2 & 0 & 0 & 0 \\ 0 & 0 & 0 & n_1^2 n_2 & n_2^3 & 2n_1 n_2^2 \end{bmatrix} \quad (47i)$$

$$[\phi_u] = \begin{bmatrix} \phi & 0 \\ 0 & \phi \end{bmatrix} \text{and } [\phi_{Du}] = \begin{bmatrix} \phi_{,1} n_1 + \phi_{,2} n_2 & 0 \\ 0 & \phi_{,1} n_1 + \phi_{,2} n_2 \end{bmatrix} \quad (47j)$$

$[S_u]$and $[S_{Du}]$ are switch matrices in the MLPG method, defined as

$[S_u] = \begin{bmatrix} S_{u1} & 0 \\ 0 & S_{u2} \end{bmatrix}$ and $[S_{Du}] = \begin{bmatrix} S_{Du1} & 0 \\ 0 & S_{Du2} \end{bmatrix}$, where

$$S_{ui} = \begin{array}{l} 1 \text{ if } u_i \text{ is prescribed on } \Gamma s_u \\ 0 \text{ if } u_i \text{ is not prescribed on } \Gamma s_u, \ i = 1,2 \end{array} \quad (47k)$$

$$S_{Dui} = \begin{array}{l} 1 \text{ if } Du_i \text{ is prescribed on } \Gamma s_{Du} \\ 0 \text{ if } Du_i \text{ is not prescribed on } \Gamma s_{Du}, \ i = 1,2 \end{array} \quad (47l)$$

$[D_\sigma]$, $[D_\tau]$and $[D_{\tau'}]$are defined respectively from following equations:

$$\{\sigma_{11}\sigma_{22}\ \sigma_{12}\}^T = [D_\sigma]\{\varepsilon_{11}\ \varepsilon_{22} 2\varepsilon_{12}\}^T \quad (47m)$$

$$\{\tau_{111}\tau_{221}\tau_{121}\tau_{112}\tau_{222}\tau_{122}\}^T = [D_\tau]\{\eta_{111}\eta_{221} 2\eta_{121}\eta_{112}\eta_{222} 2\eta_{122}\}^T \quad (47n)$$

$$\{\tau_{111,1}\ \tau_{221,1}\ \tau_{121,1}\ \tau_{112,1}\ \tau_{222,1}\ \tau_{122,1}\ \tau_{111,2}\ \tau_{221,2}\ \tau_{121,2}\ \tau_{112,2}\ \tau_{222,2}\ \tau_{122,2}\}^T = [D_{\tau'}]\{\eta_{111,1}\ \eta_{221,1}\ 2\eta_{121,1}\ \eta_{112,1}\ \eta_{222,1}\ 2\eta_{122,1}\ \eta_{111,2}\ \eta_{221,2}\ 2\eta_{121,2}\ \eta_{112,2}\ \eta_{222,2}\ 2\eta_{122,2}\}^T \quad (47o)$$

It can be easily seen that the system stiffness matrix in the present method is banded but unsymmetrical. The locations of the non-zero entries in the system 'stiffness' matrix depend upon the nodes located inside the domain of influence of the node.

5 Numerical examples

In this section, patch tests and two numerical examples, including: 1. a bimaterial system under uniform shear and 2. an infinite plane subjected to a remote uniform tension, are presented. The strain-gradient material model is as described earlier. Compared with analytical results, the MLPG method has shown its high accuracy when coping with gradient theory.

5.1 Patch test

The patch test was conducted with a known simple displacement field (Fig. 5.1)

$$\mathbf{u}(x_1, x_2) = \begin{Bmatrix} x_1 \\ x_2 \end{Bmatrix} \quad (48)$$

which satisfies the compatibility equations (2.0a, 2.0b) and governing equation (6). Also a uni-axial traction boundary problem was used in the patch test (Fig.5.2)

The formulation passed the tests for both kinds of boundary conditions, where the range of the radius of test domain varies from 1.0 to 3.5 times of the minimum nodal distanced_{min} and that of radius of support of nodal shape function varies from 3.0 to 5.0 times of d_{min} and at least one of a_i (i=1,5) in equation (4a) does not vanish. "Pass" here means that the linear displacement field (patch test 1) and the simplest (constant) conventional

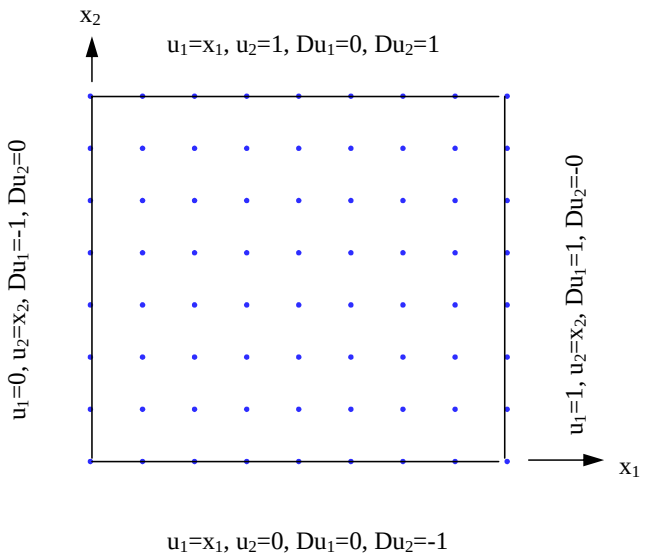

Figure 5.1: Patch test 1: essential boundary conditions are prescribed in this patch test, where the dimension of the domain in question is 1 x 1.

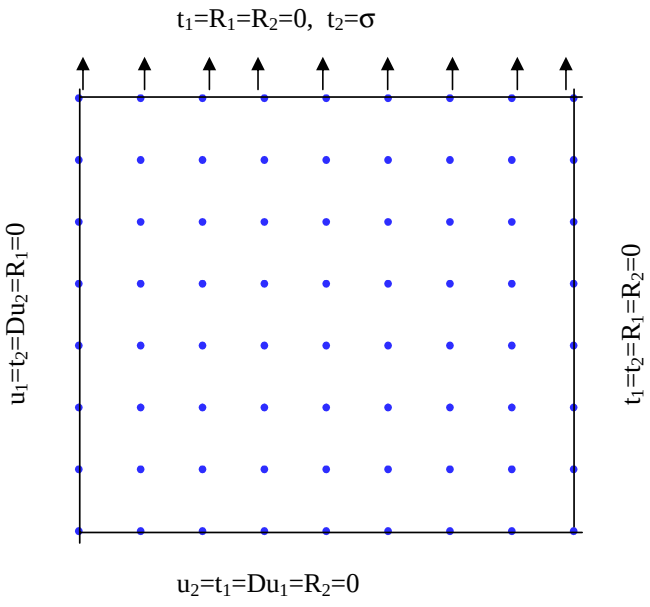

Figure 5.2: Patch test2: mixed boundary conditions are enforced, approximating the problem of an infinite plane with uni-axial traction, for the patch test.

stress field(patch test 2) were reproduced, respectively, within quadrature and roundoff errors: using double precision the maximum error in the displacement or stress field was of order 10^{-7} or 10^{-6} respectively. The main reason why a higher accuracy could not be obtained is that the shape function is very complicated and the square of the derivatives could not be integrated accurately (see Atluri and Shen, 2002a,b). So we can not expect the same accuracy in the patch test as for finite elements.

5.2 Numerical examples

Due to the complexity and difficulty of a gradient theory, the obtainable analytical solutions are only restricted to some simple problems. In this section, we will focus on two problems : 1**.** boundary layer analysis; and 2**.** the stress field analysis in an infinite plate, with a hole, subjected to bi-axial tension *p* at infinity, under a plane strain assumption.

5.2.1 Boundary layer analysis

Higher-order gradient theories predict the existence of boundary layers adjacent to in-homogeneities such as interfaces. Consider, for example, a bimaterial system composed of two perfectly bonded half planes of elastic strain gradient solids, subjected to a remote

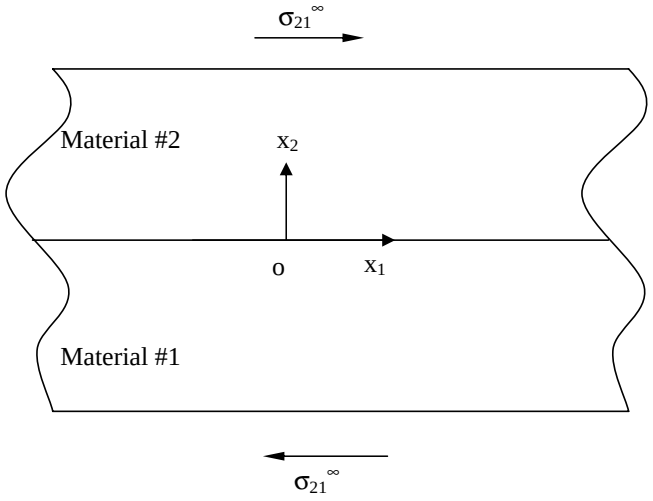

Figure 5.3: Notation and geometry of a bimaterial under uniform shear

shear stress σ_{21}^{∞} as shown in Fig. 5.3. For the strain gradient solid specified by equations (2.0-2.15) , the shear strain ε_{12} has a continuous but non-uniform distribution

within a boundary layer adjacent to the interface. In a specific quantitative example, we shall make the following arbitrary choice of constitutive parameters. The shear modulus μ of material 1 is taken to be twice that of material 2, i.e. $\mu_1 = 2\mu_2$. For each material i, the constants a_3 and a_4 (as defined in equation (4a)) are equal to $\frac{1}{2}\mu l_i^2$, $i = 1,2$, while $a_{1,}a_{2,}a_5$ vanish. Here is usually called the internal length scale for materials with strain gradient effects.

An analytical solution is presented here briefly (Shu et al. 1999). For this bimaterial system, the conventional elasticity theory dictates that the shear stress is uniform; and the shear stain jumps in magnitude at the interface, from $\varepsilon_{12} = \sigma_{12}^{\infty}/2\mu_1$ in material 1, to $\varepsilon_{12} = \sigma_{12}^{\infty}/2\mu_2$ in material 2. By including strain gradient effects, a continuously distributed shear strain can be obtained. In this problem, the only non-zero displacement, strain, stress and higher-order stress are $u_1, \varepsilon_{12}, \sigma_{12}$ and τ_{221}, respectively, and they are functions of the co-ordinate x_2 only. From the constitutive equation (4c), it follows that

$$\sigma_{12} = 2\mu_i\varepsilon_{12} \text{ and } \tau_{221} = 2\mu l_i^2\eta_{221} = 4\mu l_i^2\frac{\partial\varepsilon_{12}}{\partial x_2} \tag{49}$$

in material i. Substitution of the above relations into the governing equation (6) leads to

$$\frac{\partial\varepsilon_{12}}{\partial x_2} - \hat{l}_i^2\frac{\partial^3\varepsilon_{12}}{\partial x_2^3} = 0 \tag{50}$$

where $\hat{l}_i = \sqrt{2}l_i$. The general solution to the above ordinary differential equation is

$$\varepsilon_{12} = d_1 + d_2 e^{x_2/\hat{l}_1} \tag{51}$$

and

$$\varepsilon_{12} = d_4 + d_5 e^{x_2/\hat{l}_1} \tag{52}$$

Here d_1 to d_6 are six constants that need to be determined. The general solution is subject to the following boundary conditions:

i. $\varepsilon_{12} \to \sigma_{12}^{\infty}/2\mu_1$ as $x_2 \to -\infty$
and
$\varepsilon_{12} \to \sigma_{12}^{\infty}/2\mu_2$ as $x_2 \to +\infty$
and at the interface,

ii. continuity of traction:
$(\bar{\sigma_{12}}\tau_{221,2})|_{x_2\to 0^-} = (\bar{\sigma_{12}}\tau_{221,2})|_{x_2\to 0^+}$

iii. continuity of double stress traciton:
$\tau_{221}|_{x_2\to 0^-} = \tau_{221}|_{x_2\to 0^+}$

iv. continuity of strain: $\varepsilon_{12}|_{x_2\to 0^-} = \varepsilon_{12}|_{x_2\to 0^+}$

then the particular solution, satisfying all these conditions, is

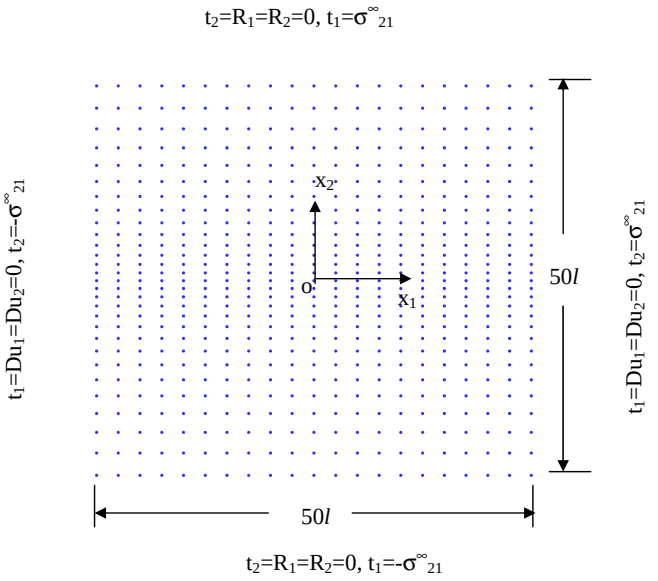

Figure 5.4: A typical nodal pattern for boundary layer analysis, where $m = 1.0$ and the uniform nodal distance in x_1 direction is $2.5l$.$x_2 < 0$ for material #1 and $x_2 > 0$ for material #2. Besides the boundary conditions shown above, we set $u_1 = u_2 = 0$ at left-bottom corner and $u_2 = 0$ at right-bottom corner to avoid the rigid movement.

$$\varepsilon_{12} = \frac{\sigma_{12}^{\infty}}{2\mu_1}\left\{1 + \frac{\mu_1 - \mu_2}{\mu_2}\frac{\mu_2\hat{l}_2}{\mu_1\hat{l}_1 + \mu_2\hat{l}_2}e^{x_2/\hat{l}_1}\right\} \text{ for } x_2 < 0 \tag{53a}$$

and

$$\varepsilon_{12} = \frac{\sigma_{12}^{\infty}}{2\mu_2}\left\{1 + \frac{\mu_2 - \mu_1}{\mu_1}\frac{\mu_1\hat{l}_1}{\mu_1\hat{l}_1 + \mu_2\hat{l}_2}e^{-x_2/\hat{l}_2}\right\} \text{ for } x_2 > 0 \tag{53b}$$

Defining $\bar{\varepsilon}_{12} = \sigma_{12}^{\infty}(\mu_1 + \mu_2)/(\mu_1\mu_2)$ as an average shear strain, solutions may be written in a dimensionless form

as

$$\varepsilon_{12}/\bar{\varepsilon}_{12} = \frac{1}{3}\left\{1+\frac{1}{3}e^{x_2/\hat{l}}\right\} \text{ for } x_2 < 0 \tag{54a}$$

$$\varepsilon_{12}/\bar{\varepsilon}_{12} = \frac{2}{3}\left\{1-\frac{1}{3}e^{-x_2/\hat{l}}\right\} \text{ for } x_2 > 0 \tag{54b}$$

where $\mu_1 = 2\mu_2$ and $l_1 = l_2 = l$ have been used without loss of generosity.

A numerical model with a typical nodal distribution is described in Fig. 5.4, where the domain with dimension of $50l$ x $50l$ is taken to model the bimaterial system. The minimum nodal distance in the x_2 direction is $m$times$l$,where the value of m varies from 0.5-3.5. Nodal distance in x_1 direction is uniform, which is 2.5 times of the minimum nodal distance in the x_2 direction.

The results are presented in Fig.5.5. The numerical solution converges quickly to the exact solution, with an increasing refinement of nodal distances, i.e. decreasing m. It is interesting to note that the strain calculated at the interface is accurate even for a very coarse nodal pattern, when m is 3.5.

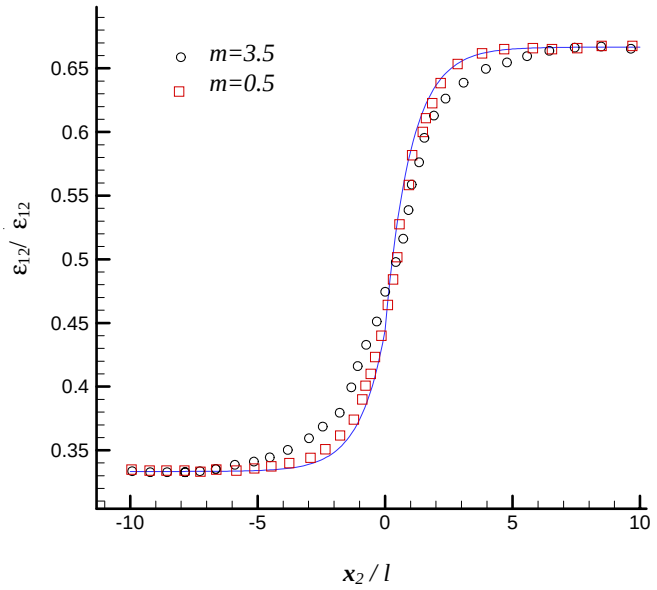

Figure 5.5: An accuracy study for various nodal patterns, where solid line denotes the analytical solution. It is noticed that a relatively coarse nodal pattern, i.e.$m = 3.5$, gives fairly accurate results. In all of these calculations, the radius of the node-based test domain (not constant) is twice that of the shortest distance from that node to other ones, i.e. $2d_{shortest}$. The radius of support of the nodal shape function is $4.5d_{shortest}$.

5.2.2 An infinite plate with a hole

The problem in section 5.2.1 could be regarded as one-dimensional problem, although it is solved in the framework of a general 2-D plane strain problem. In order to examine the convergence property of the approach in a real 2-D problem, we consider an infinite solid containing a circular cylindrical hole. The solid is subjected to a remote bi-axial uniform tension, as shown in Figure 5.6. An analytical solution was obtained (Amanatidou etc. 2002) for this problem, for the special case of a couple stress solid, i.e. the strain energy density per unit volume w depends upon strain and upon that part of strain gradients which can be expressed as

$$w = \frac{1}{2}\lambda\varepsilon_{ii}\varepsilon_{kk} + \mu\varepsilon_{ij}\varepsilon_{ij} + \frac{1}{2}l^2[\lambda\eta_{ijj}\eta_{ikk} + \mu(\eta_{ijk}\eta_{ijk} + \eta_{ijk}\eta_{kji})] \tag{55}$$

i.e. a_2, a_3 vanish in (4a) and $a_1 = \frac{1}{2}l^2\lambda,\ a_4 = a_5 = \frac{1}{2}l^2\mu$.

The problem is axially symmetric and the displacement field is of the form

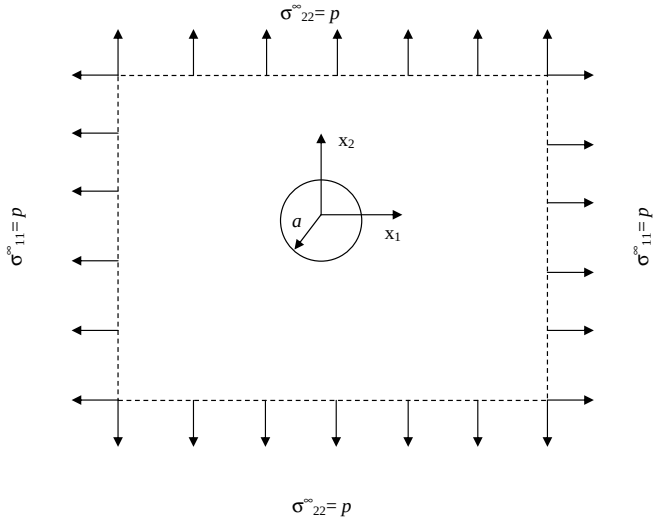

Figure 5.6: Notation and geometry of an infinite plane subjected to bi-axial remote tension.

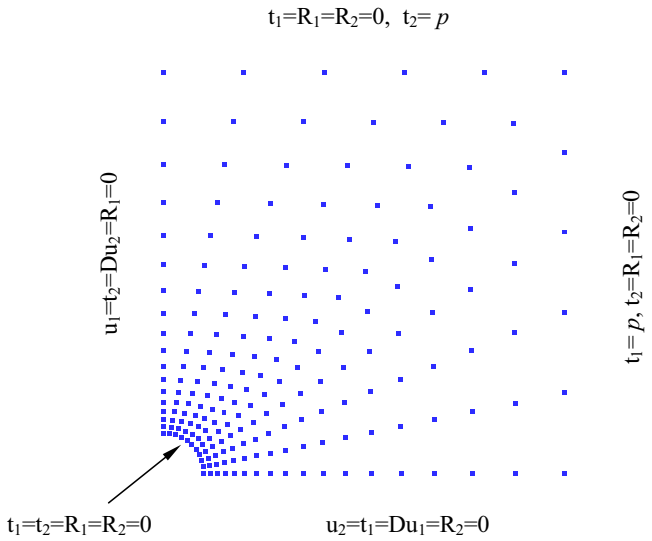

Figure 5.7: The quarter of hole in the domain is divided uniformly into 10 partitions and total number of nodes in domain is 165, where the radius of circle is a.

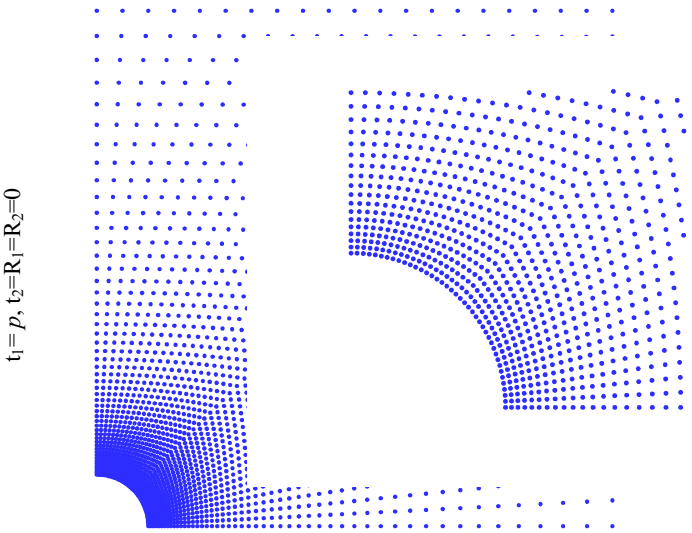

Figure 5.8: The quarter of hole in the calculated domain is divided uniformly into 40 partitions and total number of nodes in domain is 2091. The boundary conditions are as same as those in Fig.5.7.

$$u(r) = \frac{p}{2\mu}\left\{(1-2\nu)r + \frac{a^2}{r} + \frac{l}{c}\left[\frac{a}{r}K_1\left(\frac{a}{l}\right) - (1-2\nu)K_1\left(\frac{r}{l}\right)\right]\right\} \tag{56}$$

where

$$c = \frac{1-2\nu}{2}K_0\left(\frac{a}{l}\right) + \frac{1-\nu}{2}\left(\frac{4l}{a} + \frac{a}{l}\right)K_1\left(\frac{a}{l}\right) \tag{57}$$

and $K_n(x)$ are the well-known 'modified Bessel functions of the second kind'.

The problem is solved numerically using the MLPG method. One-quarter of the plate is analyzed; the nodal distributions used in the calculations are shown in Fig.5.7 and Fig. 5.8, where the total number of nodes are 165 and 2091, respectively. The numerical simulations are carried out for $\nu = 0.3$ and $a = 3l$. The domain with dimensions of $10a$ x $10a$ is taken to approximate the quarter of the infinite plate.

The following boundary conditions are prescribed (see Fig.5.7)

- $u_2 = t_1 = Du_1 = R_2 = 0$ on bottom boundary
- $u_1 = t_2 = Du_2 = R_1 = 0$ on left boundary
- $t_2 = R_1 = R_2 = 0,\ t_1 = p$ on right boundary
- $t_1 = R_1 = R_2 = 0,\ t_2 = p$ on right boundary
- $t_1 = t_2 = R_1 = R_2 = 0$ on surface of the hole

The numerical solution agrees very well with the exact solution. The displacement and stress fields are included in Fig. 5.9. and Fig. 5.10, respectively. When the total number of nodes is 2091 (shown in Fig.5.8), a remarkable accuracy is obtained. It should be noted that the classical elasticity solution with $l = 0$ predicts a stress concentration $\sigma_{\theta\theta}|_{r=a} = 2.0p$ and a value $\sigma_{rr}|_{r=a} = 0$, whereas the present gradient elasticity solution with $a = 3l$ predicts $\sigma_{\theta\theta}|_{r=a} = 1.94p$ and $\sigma_{rr}|_{r=a} = 0.16p$.

In all of these calculations, radius of node-based test-function domain (not constant) is the shortest distance from that node to other ones, i.e. $d_{shortest}$. The radius of support of the nodal shape function is around $3.0d_{shortest}$. We have noticed that increasing the node density would definitely improve the accuracy in general, but we can not blindly increase radius of test domain R_I or/and support size of nodal shape function r_I. Otherwise, numerical instability may occur.

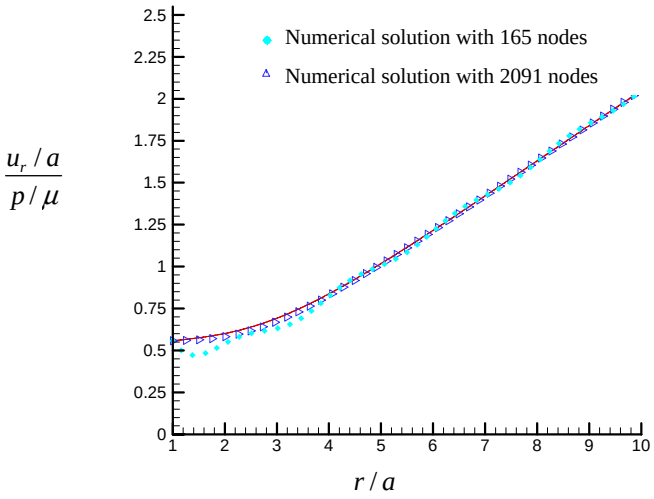

Figure 5.9: Variation of u_r for the plate with a hole, with different total number of nodes, where the solid curve denotes the exact solution.

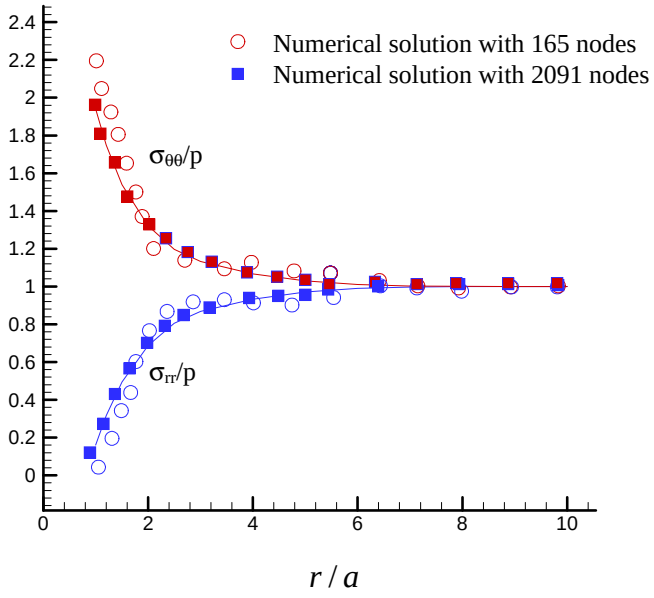

Figure 5.10: Variations of $\sigma_{\theta\theta}$and σ_{rr} for the plate with a hole, with different total number of nodes, where the solid curves denote the exact solution.

6 Concluding Remards

The Meshless local Petrov-Galerkin (MLPG) method has been developed for materials within the Toupin-Mindlin framework of strain gradient type constitutive theory. Intrinsic non-local properties of the meshless interpolation leads to real rotation-free approaches, where displacements are the only nodal degrees of freedom. The MLPG method defines the weak form of governing equations on sub-domains, which consequently helps to evaluate integration on some well-shaped region, e.g. circle in 2-D, and no mesh is needed. All of these advantages have been combined in calculations presented in this paper and quite accurate results have been obtained. The remarkable accuracy in these numerical simulations shows promising characteristics of MLPG for solving general problems of material in elasticity, where strain-gradient effects may be important.

Acknowledgement: This work is supported by NASA, and ONR, with Dr. I.S. Raja and Dr. Y.D.S. Rajapakse as the cognizant program officials. Authors also thank Dr. Z. Han for his helpful discussion and constructive suggestions.

References

E. Amanatidou and N. Aravas (2002), Mixed finite element formulations of strain-gradient elasticity problems. *Comput. Methods Appl. Mech. Engrg.* 191: 1723-1751

S.N Atluri, T. Zhu (1998a): A new meshless local Petrov-Galerkin(MLPG) approach to nonlinear problems in com-putational modeling and simulation. *Comput. Modeling Simulation in Engrg.* 3: 187-196

S.N Atluri, T. Zhu (1998b): A new meshless localPetrov-Galerkin (MLPG) approach in computational mechanics. *Comput. Mech.* 22: 117-127

S.N Atluri, JY Cho, HG **Kim** (1999): Analysis of thin beams, using the meshless local Petrov-Galerkin method, with generalized moving least squares interpolations. *Comput. Mech.* 24: 334-347

0A**S.N Atluri, HG Kim , JY Cho** (1999): A critical assessment of the truly meshless local Petrov-Galerkin(MLPG) and local boundary integral equation (LBIE)methods. *Comput. Mech.* 24: 348-372

S.N Atluri., J. Sladek , V. Sladek , T. Zhu (2000): The local boundary integral equation (LBIE) and it's mesh-

less implementation for linear elasticity. *Comput. Mech.* 25:180-198

S.N Atluri, T. Zhu (2000): The meshless local Petrov-Galerkin(MLPG) approach for solving problems in elasto-statics, *Comput. Mech.* 25: 169-179

S.N Atluri, T. Zhu (2000): New concepts in meshless methods. *Int. J. Numer. Mech. Engrg.* 47: 537-556

S.N Atluri (2002): Methods of computer modeling in engineering and sciences. Tech. Science Press, 1400 pages.

S.N Atluri, S. Shen(2002a), The Meshless Local Petrov-Galerkin (MLPG) Method: A Simple & Less-costly Alternative to the Finite Element and Boundary Element Methods, *CMES: Computer Modeling in Engineering & Science*, vol.3, no.1: 11-51

S.N Atluri, S. Shen (2002b): *The meshless local Petrov-Galerkin(MLPG) metho*d. Tech. Science Press.

I. Babuka and **M. Zlámal** (1973), Nonconforming elements in the finite element method with penalty SIAM *Journal on Numerical Analysis*, 10: 863-875.

G.A. Baker (1977), Finite element methods for elliptic equations using nonconforming elements. *Mathematics of Computation* 31 (137) : 45-59.

R. de Borst and **L.J. Sluys** (1991), Localisation in a cosserat continuum under static and dynamic loading conditions. *Computer Methods in Applied Mechanics and Engineering*, 90: 805-827.

I. Babuska, JM Melenk (1997): The partition of unity method. *Int. J. Num. Meth. Engrg.* 40: 727-758

T. Belytschko , YY Lu, L. Gu (1994): Element-free Galerkin methods. *Int. J. Num. Meth. Engrg.* 37: 229-256

T. Belytschko, Y. Krongauz, D. Organ, M. Fleming, P. Krysl (1996): Meshless methods: An overview and recent developments. *Comput. Methods Appl. Mech.Engrg.* 139: 3-47

A.L. Cauchy (1851), Note sur léquilibre et les mouvements vibratoires des corps solids. *Comptes Rendus de I'Academie des Sciences. Serie I, Mathématique* 32 (1851): 323-326.

J. Chen, **H. Yuan** and **F.H. Wittmann** (2002), Computational Simulations of Micro-Indentation Tests Using Gradient Plasticity, *CMES: Computer Modeling in Engineering & Science*, Vol.3, No.6 : 743-754

E. Cosserat and **F. Cosserat** (1907), Sur la mécanique génerale. *Comptes Rendus de I'Academie des Sciences, Serie I, Mathématique* 145 : 1139-1142.

E. Cosserat and **F. Cosserat** (1909), Theorie des Corps Déformables. , Hermann, Paris .

HK Ching, RC Batra (2001): Determination of Crack Tip Fields in Linear Elastostatics by the Meshless Local Petrov-Galerkin (MLPG) Method. *CMES: Computer Modeling in Engineering & Sciences* 2 (2): 273-290

C. Duarte , JT Oden (1996): Hp-cloud – a meshless method to solve boundary-value problems. *Comput. Meth. Appl. Mech. Eng.* 139: 237-262

G. Engel, **K. Garikipati**, **T.J.R. Hughes**, **M.G. Larson**, **L. Mazzei**, and **R.L. Taylor**, (2002), Continuous/discontinuous finite element approximations of fourth-order elliptic problems in structural and continuum mechanics with applications to thin beams and plates, and strain gradient elasticity, *Comput. Methods Appl. Mech. Engrg.* 191 : 3669-3750

A.C. Eringen (1976), Continuum Physics, vol. 4: Polar and Nonlocal Field Theories. , New York, Academic Press.

N.A. Fleck, **G.M. Muller**, **M.F. Ashby** and **J.W. Hutchinson** (1994), Strain gradient plasticity: theory and experiment. *Acta Metallurgica et Materialia*, 42 : 475-487

N.A. Fleck and **J.W. Hutchinson** (1997), Strain gradient plasticity. *Advances in Applied Mechanics* 33: 295-361.

H. Gao, **Y. Huang** and **W.D. Nix** (1999), Mechanism-based strain gradient plasticity. I. Theory. *Journal of the Mechanics and Physics of Solids* , 47: 1239-1263.

RA Gingold, JJ Monaghan (1977): Smoothed particle hydrodynamics: theory and application to non-spherical stars. *Mon. Not. Roy. Astron. Soc.* 181:375-389

YT Gu, GR Liu (2001): A meshless local Petrov-Galerkin (MLPG) formulation for static and free vibration analysis of thin plates. *CMES: Computer Modeling in Engineering & Sciences* 2 (4): 463-476

L. R.Herrmann (1983), Mixed finite elements for couple-stress analysis, in Atluri, S. N. , Gallagher, R. H. and Zienkiewicz, O. C. (eds.), Hybrid and Mixed Finite Element Methods, Wiley, New York.

Y. Huang, **H. Gao**, **W.D. Nix** and **J.W. Hutchinson** (2000), Mechanism-based strain gradient plasticity. II. Analysis. *Journal of the Mechanics and Physics of Solids*, 48: 99-128

W.K. Liu, Y. Chen, R.A. Uras, C.T. Chang (1996): Generalized multiple scale reproducing kernel particle methods. *Comput. Methods Appl. Mech. Engrg.* 139: 91-157

S. Long and **S. Atluri** (2002): A meshless local Petrov-Galerkin Method for Solving the Bending Problem of a Thin Plate, *CMES: Computer Modeling in Engineering & Science*, vol.3, no.1: 53-63, 2002

R. D. Mindlin, (1963) Influence of couple-stresses on stress concentrations, *Exp. Mech.* , 3: 1-7 .

R.D. Mindlin (1964), Micro-structure in linear elasticity. *Archive for Rational Mechanics and Analysis* , 16, 51-78.

B Nayroles, G Touzot, P Villon (1992): Generalizing the finite element method: diffuse approximation and diffuse elements. *Comput. Mech.* 10: 307-318

E. Oñate and **M. Cervera** (1993), Derivation of thin plate bending elements with one degree of freedom per node: a simple three node triangle. *Engineering Computations*, 10 (6): 543-561.

E. Oñate and **F. Zarate** (2000), Rotation-free triangular plate and shell elements. *International Journal for Numerical Methods in Engineering*, 47 (1): 557-603.

R. Phaal and **C.R. Calladine** (1992), A simple class of finite-elements for plate and shell problems. 1. Elements for beams and thin flat plates. *International Journal for Numerical Methods in Engineering* ,35 (5): 955-977.

R. Phaal and **C.R. Calladine** (1992), A simple class of finite-elements for plate and shell problems. 2. An element for thin shells with only translational degrees of freedom. *International Journal for Numerical Methods in Engineering* 35 (5): 979-996.

D. Shepard (1968): A two-dimensional function for irregularly spaced points. *Proc. Of ACM Nat'l Conf.*: 517-524

J. Y. Shu, and **N. A Fleck**(1998), Prediction of a size effect in micro indentation, *Int. J. Solids Struct.* , 35: 1363-1383 .

J.Y. Shu, **W.E. King** and **N.A. Fleck** (1999), Finite elements for materials with strain gradient effects. *International Journal for Numerical Methods in Engineering* , 44: 373-391.

B. Specht (1988), Modified shape functions for the three node plate bending element passing the patch test, *Int. J. Numer. Meth. Engng.*, 26: 705-715

N.A. Stelmashenko, **M.G. Walls**, **L.M. Brown** and **Y.V. Milman**(1993) , Microindentation studies on W and Mo oriented single crystals. *Acta Metallurgica et Materialia*, 41: 2855-2865.

J.S. Stolken and **A.G. Evans** (1998), Microbend test method for measuring the plasticity length scale. *Acta Materialia*, 46: 5109-5115

G. Strang and **G.J. Fix** (1973), An Analysis of the Finite Element Method. , Prentice-Hall, Englewood Cliffs, NJ.

N. Sukumar , B. Moran , T. Belytschko (1998): The natural element method in solid mechanics. *Int. Num. Meth. Eng.* 43: 839-887

L.T. Tenek and **E.C. Aifantis**(2002), A Two-dimensional Finite Element Implementation of a Special Form of Gradient Elasticity, *CMES: Computer Modeling in Engineering & Science*, Vol.3, No.6: 731-742

S. Timoshenko and **S. Woinowsky-Krieger**(1959) , Theory of Plates and Shells. (second ed.),, McGraw-Hill, New York.

R.A. Toupin(1962) , Elastic materials with couple-stresses. *Archive for Rational Mechanics and Analysis* , 11: 385-414

C. Truesdell and **R.A. Toupin** (1960), Principles of classical mechanics and field theory. In: Handbuch der Physik vol III/1, Springer, Berlin.

C. Truesdell and **W. Noll**(1965) , The non-linear field theories of mechanics. In: Handbuch der Physik vol. III/3, Springer, Berlin.

H. Wendland (1995): Piecewise polynomial, positive definite and compactly supported radial basis functions of minimal degree. *Adv. Comput. Math.* 4:389-396

H. Wendland (1998): Error estimates for interpolation by compactly supported radial basis functions of minimal degree. *J. Approx. Theory* 93: 258-272

H. Wendland (1999): Meshless Galerkin methods using radial basis function. *Math. Comput.* 68(228): 1521-1531

Z.C. Xia, and J. W **Hutchinson** (1996), Crack tip fields in strain gradient plasticity, *J. Mech. Phys. Solids* , 44: 1621-1648.

O. C. Zienkiewicz, and R. L.**Taylor**, The Finite Element, 4th edn., McGraw-Hill, New York, 1994